Electron-Nuclear Coupling to the Proximal Histidine in Oxy Cobalt-Substituted Distal Histidine Mutants of Human Myoglobin†

H. Caroline Lee*,‡ and Jack Peisach‡,§

Departments of Molecular Pharmacology and of Physiology and Biophysics, Albert Einstein College of Medicine of Yeshiva University, Bronx, New York 10461

Yi Dou and Masao Ikeda-Saito

Department of Physiology and Biophysics, Case Western Reserve University School of Medicine, Cleveland, Ohio 44106-4970

Received February 8, 1994; Revised Manuscript Received April 14, 1994®

ABSTRACT: Electron spin echo envelope modulation (ESEEM) spectroscopy was used to investigate electron-nuclear coupling to the N_ϵ of the proximal histidine (F8, His 93) imidazole in oxyCo(II)-substituted distal histidine (E7, His 64) mutants (His → Leu, His → Val, His → Gly, His → Gln) and recombinant wild-type human myoglobins (Mbs). Nuclear hyperfine and nuclear quadrupole coupling constants decrease in the order: H64L > H64V ≥ H64G ≈ H64Q > wild-type. The differences in couplings found for the four mutant proteins are correlated with the differences in polarity of the E7 side chain. On the basis of the relative orientation of the nuclear quadrupole and *g* tensors, obtained by computer simulation of ESEEM spectra, the Co–O–O bond angle of H64G and H64Q appears to be similar to that of oxyCo sperm whale Mb (and possibly wild-type human Mb) at room temperature [Hori et al. (1982) *J. Biol. Chem. 257*, 3636], while that in H64V and H64L is more obtuse. ESEEM measurements in D_2O demonstrate the presence of a hydrogen bond between the distal histidine and bound O_2 in the wild-type protein, as was found in oxyCo sperm whale and horse Mbs [Lee et al. (1992) *Biochemistry 31*, 7274]. This hydrogen bond leads to a reduction in the N_ϵ coupling in the wild-type protein as compared to that in the E7 mutants. No hyperfine-coupled deuterons were found in any of the mutants, and therefore, the proposed hydrogen bond between bound O_2 and the distal glutamine in H64Q [Ikeda-Saito et al. (1991) *J. Biol. Chem. 266*, 23641] could not be substantiated.

The proximal histidyl imidazole, the endogenous axial ligand of heme iron, is conserved in most O_2-carrying hemoproteins including human Mb[1] (Hunt et al., 1978; Dickerson & Geis, 1983). In oxy globins, the heme iron–proximal His bond can be affected by interactions between bound O_2 and nearby amino acids in the distal heme pockets, interactions such as those altering the basicity of the bound O_2 and/or the geometry of the Fe–O–O bonds. However, these *trans* effects of the O_2 on the proximal His ligand can seldom be investigated in a straightforward manner. For example, EPR spectroscopy cannot be applied to oxyferrous globins since the metal center is diamagnetic (Savicki et al., 1984). The resonance Raman frequency of the Fe–proximal His bond has yet to be identified in ligated ferrous globins (Yu, 1987), while proton resonances of the proximal His in ligated ferrous Mb have been reported only for the CO-bound form of the protein (Dalvit & Wright, 1987).

Co substitution for Fe provides an avenue for the investigation of the metal–proximal His bond in oxy globins using ESEEM spectroscopy. Co-substituted globins, functional analogues of the ferrous proteins (Hoffman & Petering, 1970), are paramagnetic, with the unpaired electron in the $S = 1/2$ metal center residing primarily in an antibonding π^* orbital of the O_2 ligand (Hoffman et al., 1970; Dedieu et al., 1976; Tovrog et al., 1976). Electron-nuclear hyperfine coupling to the N_ϵ of the proximal histidyl imidazole, believed to occur via spin polarization of the fully occupied σ orbital $N_{sp^2} + Co_{dz^2} + \pi^*(O_2)$ (Wayland & Abd-Elmageed, 1974), is too small to be observed by CW EPR but can be measured by ESEEM spectroscopy (Magliozzo et al., 1987; Lee et al., 1992). This coupling can be modulated by perturbation of the Co–O_2 bond so that distal effects at or near the bound O_2 are propagated through Co. ESEEM studies of oxyCo globins also provide information on nuclear quadrupole coupling to the proximal histidyl N_ϵ. This parameter is related to the extent of donation of the lone-pair electrons to Co (Magliozzo et al., 1987) and is therefore a direct measurement of the extent of the overlap of the Co d_{z^2} orbital and the N_ϵ lone-pair-containing sp^2 hybrid in a way reflecting the Co–imidazole bond strength.

The focus of previous ESEEM studies of various oxy Co-substituted globins (Lee et al., 1992, 1993) has been to ascertain the effect of hydrogen bonding between bound O_2 and the histidyl imidazole in the distal heme pocket on electron-nuclear coupling to the N_ϵ of the proximal His. In the present investigation, other mechanisms by which the distal His modulates the *trans* effect of the bound O_2 on the proximal His coupling are examined, using human Mb mutants where

† This work was supported by N.I.H. Grants GM40168 (J.P.), RR02538 (J.P.), GM39492 (M.I.-S.), and RR05659 (M.I.-S.) and a grant-in-aid from the Northeast Ohio Affiliate of the American Heart Association (M.I.-S.). It is dedicated to the memory of Professor Masao Kotani.

* Author to whom correspondence should be addressed.

‡ Department of Molecular Pharmacology.

§ Department of Physiology and Biophysics.

® Abstract published in *Advance ACS Abstracts,* June 1, 1994.

[1] Abbreviations: acacen, acetylacetonatiminato; CW, continuous wave; efg, electric field gradient; EPR, electron spin resonance; ESEEM, electron spin echo envelope modulation; Mb, myoglobin; N-MeIm, *N*-methylimidazole; NMR, nuclear magnetic resonance; NQI, nuclear quadrupole interaction; PPIX, protoporphyrin IX; py, pyridine; TPivP, *meso*-tetrakis(α,α,α,α-*o*-pivalamidophenyl)porphyrin, "picket fence" porphyrin; TPP, tetraphenylporphyrin.

0006-2960/94/0433-7609$04.50/0

the distal His (His^{64,E7}) has bee replaced by a Leu, Val, Gln, or Gly residue. Substitution of these amino acids at position E7 in sperm whale Mb has been found to affect O_2-dissociation kinetics of the oxyferrous proteins (Olson et al., 1988; Rohlfs et al., 1990; Carver et al., 1990), albeit to varying degree. This suggest that the Fe–O_2 bond strength is different in each sperm whale Mb mutant and that the Fe–proximal His bond may, in turn, be affected differently. A comparable scenario is envisioned for the analogous human Mb mutants.

This paper presents ESEEM studies of oxyCo-substituted Mb(H64L), -(H64Q), -(H64V), and -(H64G) and wild-type protein[2] in order to investigate the relationship between the nature of the distal E7 residue and the Co–proximal His interaction. Computer simulation of spectra is used to obtain nuclear hyperfine and nuclear quadrupole coupling parameters. An estimate of the relative orientations of the g, ^{14}N nuclear hyperfine, and ^{14}N nuclear quadrupole tensors provides information on the Co–O–O bond angle and the relative orientation of the O–O bond with respect to the heme plane. These results demonstrate the effect of the E7 side-chain polarity and volume on the electronic structure of the O_2–Co–His unit.

This paper also presents ESEEM studies of the various oxyCo Mb mutants in D_2O in order to detect exchangeable deuterons in the vicinity of the bound O_2 and to differentiate signals arising from ambient deuterons from those that are hyperfine-coupled, for example, through hydrogen bonding (Lee et al., 1992, 1993), to the unpaired electron on O_2. D_2O-induced narrowing of the Co hyperfine features in CW EPR spectra has been used as a probe for hydrogen bonding between the distal His and bound O_2 in oxyCo globins (Yonetani et al., 1974a; Ikeda-Saito et al., 1978, 1981). Similar D_2O effects have been observed in the EPR spectra of H64Q, H64V (Ikeda-Saito et al., 1991), and H64G (Dou et al., unpublished data). It is noteworthy that the latter two mutants are not expected to contain a hydrogen bond to bound O_2. For H64Q, a hydrogen bond to bound O_2 is possible (Ikeda-Saito et al., 1991), based on analogy with elephant Mb where a hydrogen bond between the E7 glutamine and O_2 has been proposed (Krishnamoorthi et al., 1984).

Our ESEEM studies detect hyperfine-coupled deuteron only in the wild-type protein, thus demonstrating the presence of a hydrogen bond to bound O_2, as was found in oxyCo sperm whale and horse Mb (Lee et al., 1992). This strongly suggests that the distal pocket structure of the recombinant wild-type protein is identical to that of native human Mb. On the other hand, the proposed hydrogen bond between the E7 glutamine and bound O_2 in H64Q (Ikeda-Saito et al., 1991) cannot be substantiated.

MATERIALS AND METHODS

Protein Preparation. Preparation of recombinant human Mbs and substitution of the heme with CoPPIX have been described previously (Ikeda-Saito et al., 1991). Preparation of Co-substituted Mb(H64Q) followed the procedure of Yonetani et al. (1974b). No ion-exchange chromatography was conducted following the Sephadex column chromatography.

Samples for EPR and ESEEM measurements were prepared by mixing one part (v/v) protein with two parts buffer. The buffers used were 0.1 M HEPES, pH 7, in H_2O or D_2O (90 atom %), such that the final concentration of deuterium in D_2O samples was 60 atom % (also see Results). pH meter readings were not corrected for isotope effects. Oxygenated samples of the wild-type protein were prepared in air. For the mutants, protein was mixed with oxygenated buffer and the samples were allowed to equilibrate with oxygen at 0 °C before freezing in liquid nitrogen (Ikeda-Saito et al., 1991). CW EPR measurements indicated that all samples were fully oxygenated. Final protein concentrations were 0.6–0.8 mM.

Spectroscopy. CW EPR spectra were obtained at 77 K on a Varian E112 spectrometer equipped with a Systron-Donner frequency counter.

ESEEM data were recorded at liquid helium temperatures (1.4–4.2 K) on a pulsed EPR spectrometer described previously (McCracken et al., 1987), using folded stripline cavities (Britt & Klein, 1987) that can accommodate 4-mm, o.d., EPR tubes. Three pulse, or stimulated echo, experiments (Peisach et al., 1979) were conducted at microwave frequencies between 8.5 and 10.1 GHz. The time interval between the first and second microwave pulses, τ, was chosen as multiples of the proton Larmor frequency in order to suppress modulations from weakly coupled ^1H (Peisach et al., 1979). Data were collected at the time $2\tau + T$, where T was the time interval between the second and third pulses. Each data set contained 1024 points; each point represented the average of 250 measurements of the intergrated electron spin echo. The spectra presented are Fourier transformations of the time domain data subsequent to dead time reconstruction (Mims, 1984).

Computer Simulation. CW EPR spectra were simulated using a modifed version of the program QPOWA (Belford & Nilges, 1979; Nilges, 1981; Maurice, 1981) with line widths of 25, 15, and 15 MHz in the x, y, and z directions, respectively. Spectra of D_2O-exchanged samples were normally used as references for the simulations because of the improved resolution of ^{59}Co hyperfine lines in this solvent.

The computer program for simulation of ESEEM spectra has been described previously (Cornelius et al., 1990). The input parameters for a simulation are (i) the principal values of the g and ^{59}Co ($I = {}^7/_2$) nuclear hyperfine tensors, obtained from simulation of frozen solution CW EPR spectra, except in the case of the wild-type protein (see Results), (ii) the experimental parameters including microwave frequency, magnetic field strength, and the τ value, and (iii) the parameters for the ^{14}N spin Hamiltonian:

$$\hat{\mathbf{H}}_N = -g_N\beta_N\mathbf{B}I + S\mathbf{A}_N I + (e^2qQ/4)[3I_z2 + 2 + \eta(I_x2 - I_y2)] \quad (1)$$

where $\mathbf{B}$ is the magnetic field, S and I are the electron spin and nuclear spin operators, and β is the Bohr magnetron. The first, second, and third terms of eq 1 represent the nuclear Zeeman, nuclear hyperfine, and nuclear quadrupole interactions. The nuclear hyperfine tensor, $\mathbf{A}_N$, is taken to be axial, with principal values $A_{iso} - F$, $A_{iso} - F$, $A_{iso} + 2F$ (Cornelius et al., 1990). A_{iso} is the isotropic nuclear hyperfine coupling constant, $F = g_N\beta_N g_e\beta_e/(r_{eff})^3$ is the anisotropic coupling constant, and r_{eff} is the effective dipole distance. Two angles, θ_N and ϕ_N, relate the orientation of the nuclear hyperfine and g tensors. The NQI is described by a nuclear quadrupole coupling constant, e^2qQ, and an asymmetry factor, η, which

[2] Unless otherwise specified, the abbreviation H64L, etc., and the term wild-type used in this paper refer to the oxy Co-substituted recombinant human Mb and not the iron protein.

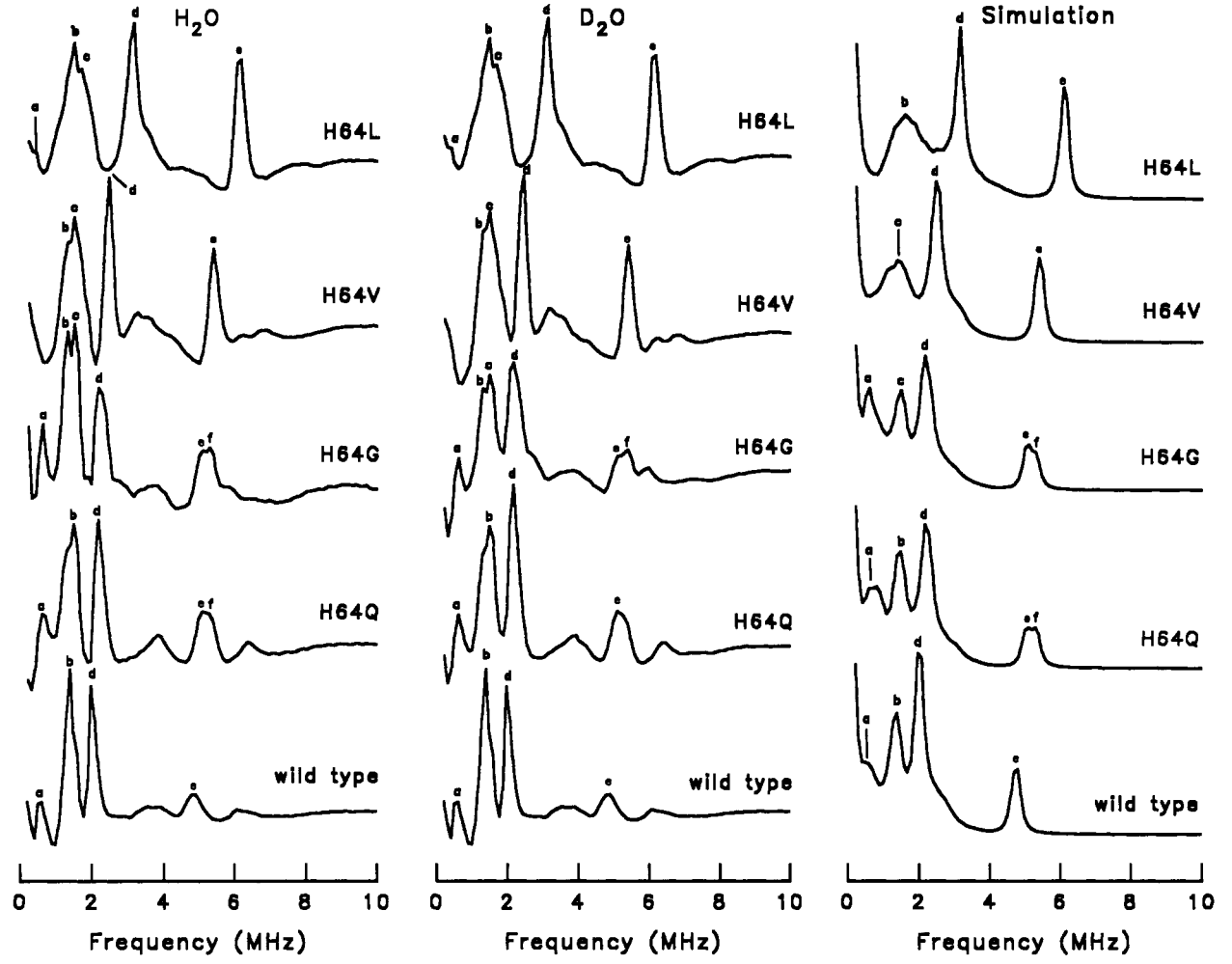

FIGURE 1: ESEEM spectra of oxyCo mutant and wild-type human Mb in 0.67 mM Hepes, pH 7, in H_2O (left panel), in D_2O (middle panel), and simulation (right panel). Labeled peak positions are summarized in Table 1. Experimental conditions for the H_2O spectra of H64L are microwave frequency = 8.50 GHz, magnetic field = 2992 G, τ = 157 ns, temperature = 4.2 K; for H64V, microwave frequency = 8.51 GHz, magnetic field = 2997 G, τ = 157 ns, temperature = 1.4 K; for H64G, microwave frequency = 8.47 GHz, magnetic field = 3029 G, τ = 155 ns, temperature = 1.4 K; for H64Q, microwave frequency = 8.54 GHz, magnetic field = 3067 G, τ = 153 ns, temperature = 4.2 K; and for the wild-type, microwave frequency = 8.54 GHz, magnetic field = 3006 G, τ = 156 ns, temperature = 4.2 K. Experimental conditions for the D_2O spectra of H64L are microwave frequency = 8.50 GHz, magnetic field = 2992 G, τ = 157 ns, temperature = 4.2 K; for H64V, microwave frequency = 8.64 GHz, magnetic field = 3041 G, τ = 155 ns, temperature = 1.4 K; for H64G, microwave frequency = 8.65 GHz, magnetic field = 3112 G, τ = 151 ns, temperature = 1.4 K; for H64Q, microwave frequency = 8.54 GHz, magnetic field = 3066 G, τ = 153 ns, temperature = 4.2 K; and for the wild-type, microwave frequency = 8.54 GHz, magnetic field = 3006 G, τ = 156 ns, temperature = 4.2 K. Simulation parameters are summarized in Table 3.

are related to the principal values (q_{xx}, q_{yy}, q_{zz}) of the electric field gradient tensor by:

$$e^2qQ = e^2q_{zz}Q \quad (2)$$

$$\eta = (q_{yy} - q_{xx})/q_{zz} \quad (3)$$

where $|q_{zz}| > |q_{yy}| > |q_{xx}|$. Three Euler angles, α, β, and γ, relate the orientations of the NQI and the g tensors. In a typical simulation, input parameters for ^{14}N nuclear hyperfine and NQI are varied until reasonable fits are obtained for data collected at three experimental g values (1.99, 2.03, 2.08).

All simulations were performed on a Microvax II computer.

RESULTS

ESEEM of OxyCo Mb Mutants and Computer Simulation of Spectra. The ESEEM spectra of oxyCo mutant and wild-type Mb (Figure 1, left panel) arise from electron-nuclear coupling to the directly coordinated N_ϵ of the proximal histidyl imidazole (Lee et al., 1992). These are characteristic spectra of an $S = 1/2$ system with a weakly coupled ^{14}N ligand (Mims & Peisach, 1978). The ESEEM spectrum of the wild-type protein (Figure 1, left panel), identical to those of oxyCo sperm whale and horse Mb (Lee et al., 1992), is typical for a coupled ^{14}N at the condition of "exact cancellation" (Flanagan & Singel, 1978), often observed for the remote (amino) nitrogen of ligated imidazole in Cu(II)–imidazole complexes and Cu(II) proteins (Mims & Peisach, 1978; Jiang et al., 1990). Here, the magnitude of the nuclear Zeeman interaction is approximately half of that of the nuclear hyperfine interaction (eq 1) such that in one of the electron spin manifolds, they cancel each other. The ESEEM spectrum, then, consists of three sharp low-frequency lines, with the frequencies of the first two (ν_0, ν_-) adding to give the third (ν_+). These are the "zero field" quadrupole resonance lines, and their frequencies are related to the nuclear quadrupole coupling constant e^2qQ and the asymmetry factor η by:

$$\nu_\pm = 3/4e^2qQ(1 \pm \eta/3) \quad (4)$$

$$\nu_0 = 1/2e^2qQ\cdot\eta \quad (5)$$

The spectrum also contains a fourth, broad, high-frequency

Table 1: Peak Positions for Spectra Shown in Figure 1

	peak position (MHz)					
sample	a	b	c	d	e	f
			H_2O			
H64L	0.30	1.45	1.63	3.12	6.14	
H64V		1.30	1.45	2.43	5.36	
H64G	0.58	1.26	1.45	2.13	5.08	5.27
H64Q	0.58	1.45		2.13	5.06	5.27
wild-type	0.56	1.36		1.93	4.77	
			D_2O			
H64L	0.30	1.45	1.63	3.12	6.14	
H64V		1.30	1.45	2.43	5.36	
H64G	0.58	1.26	1.45	2.13	5.08	5.27
H64Q	0.58	1.45		2.13	5.06	
wild-type	0.56	1.36		1.93	4.77	
			simulation			
H64L		1.57		3.12	6.14	
H64V			1.44	2.43	5.36	
H64Q	0.58		1.45	2.16	5.07	5.24
H64Q	0.58	1.44		2.16	5.01	5.26
wild-type	0.56	1.36		1.93	4.77	

line which arises from the second electron spin manifold where the nuclear Zeeman interaction adds to the nuclear hyperfine interaction, resulting in a $\Delta m_I = 2$ transition (Mims & Peisach, 1978). With small anisotropy in the hyperfine coupling, the frequency of this broad line is close to twice the isotropic hyperfine coupling constant A_{iso} or 4 times the ^{14}N nuclear Zeeman energy at the experimental magnetic field.

For an ^{14}N not at exact cancellation, computer simulation of spectra can be used to obtain the nuclear hyperfine and nuclear quadrupole coupling parameters. In simulations of frozen solution data, the g tensor, instead of the molecular axes, is used as the reference frame, making it desirable to obtain a precise set of g values. For the four mutants, this is achieved by computer simulation (Figure 2, right panel) of frozen solution CW EPR spectra (Ikeda-Saito et al., 1991) (Figure 2, left panel). For the wild-type protein, the g values obtained from a single-crystal EPR study of oxyCo sperm whale Mb (Hori et al., 1982) are used, since the human wild-type protein exhibits a frozen solution EPR spectrum (Ikeda-Saito et al., 1991) identical to that of oxyCo sperm whale Mb (Yonetani et al., 1974a).[3] EPR parameters are summarized in Table 2.

In a typical simulation of an ESEEM spectrum, the coupling parameters A_{iso}, e^2qQ, η, and, to a smaller extent, r_{eff} are first varied to obtain a frequency match for data collected at $g = 2.03$. The angles β (θ_N) (see below) and α are then varied in steps of 10° (with adjustment of the coupling parameters obtained for the $g = 2.03$ setting) to obtain fits for data collected at two other g values (1.99, 2.08). The criteria for determining a set of angles are as follows. The angles should (i) best produce the general shape of the low-frequency region of the ESEEM spectrum obtained at different g values, a region sensitive to variations of the Euler angles, and (ii) require the least adjustment of the coupling parameters to fit data at different g values. The range of parameters used in fitting spectra collected at different g values (using a single set of angles) defines the uncertainties[4] in the simulations.[5] Since the hyperfine tensor is assumed to be axial (see Materials and Methods), A_{xx}^N and A_{yy}^N can be along any direction in the xy plane, so an angle of $\phi_N = 0°$ is assumed. Variation of ϕ_N is found to have almost no effect on the simulations. An input γ of >40° changes the relative intensities of the spectral components but does not lead to an improvement in the fits. Therefore, this angle is taken to be 0° in simulations presented in this paper. Simulated ESEEM spectra are shown in Figure 1, right panel. Coupling parameters are summarized in Table 3. Hyperfine and quadrupole coupling parameters increase in the order: wild-type < H64Q ≈ H64G ≤ H64V < H64L. Simulations for H64L and H64V require small values for β, θ_N, and α, while for H64G and H64Q, larger values for β, θ_N, and α are needed.

The Euler angles α, β, and γ and the polar angles θ_N and ϕ_N define the relative orientations of the ^{14}N nuclear quadrupole and nuclear hyperfine tensors, respectively, with respect to the g tensor and contain information on molecular structure (Jiang et al., 1993). In the absence of an X-ray crystal structure and a single-crystal EPR study, as in the case of the mutants, it is still possible to correlate magnetic tensor orientations with molecular structure if reasonable reference systems are available. Figure 3 illustrates how the relative orientations of the three magnetic tensors of the oxyCo mutants can be correlated with their molecular structures. The g tensors of all the mutants are assumed to be analogous to that of oxyCo sperm whale Mb and are defined by the O–O bond direction (Petsko et al., 1978; Hori et al., 1980, 1982).[6] g_z (g_{min}) is directed along the O–O bond, and g_x (g_{max}) is along the unpaired electron-containing π^* orbital of O_2. A_{zz}^N is assumed to be along the Co–N_ϵ(His) bond, since hyperfine coupling to ^{14}N is believed to arise from spin polarization of the N_ϵ–Co–O_2 σ orbital (Wayland & Abd-Elmageed, 1974). q_{zz} is taken to be along the N_ϵ(His) lone-pair-containing sp^2 hybrid and q_{yy} along the N_ϵ $p\pi$ orbital, perpendicular to the imidazole plane (Hsieh et al., 1977; Ashby et al., 1978).[7] The quadrupole tensor therefore coincides with the hyperfine tensor, as was demonstrated in an ESEEM study of oxyCoTPP models (Magliozzo et al., 1987). For this reason, $\beta(q_{zz} \wedge g_z)$[8] $= \theta_N(A_{zz}^N \wedge g_z)$[8] is assumed in all the simulations, and these angles may reflect the Co–O–O bond angle in the protein. The projection of the O–O bond on the porphyrin plane determines the angle $\alpha(q_{yy} \wedge g_y)$.[8] In oxyCo sperm whale Mb (Phillips, 1980; Hori et al., 1980, 1982),[6] the projection of the O–O bond on the porphyrin plane is along the porphyrin N_I–

[3] The frozen solution EPR spectrum of the oxyCo wild-type Mb has been proposed to contain two signals (Ikeda-Saito et al., 1991), as in the case of the single-crystal EPR spectrum of oxyCo sperm whale Mb (Chien & Dickinson, 1972; Dickinson & Chien, 1980; Hori et al., 1980, 1982). The reported g and A^{Co} values of both species I and II of oxyCo sperm whale Mb given by Hori et al. (1980, 1982) are used in the simulation of the ESEEM spectrum of the wild-type.

[4] The range in simulation parameters is 0.03–0.10 MHz for A_{iso}, with the largest range found for H64V, 0.02–0.09 MHz for e^2qQ, with the largest found for H64G, and 0.03–0.33 for η, with the largest found for H64V (also see text).

[5] The width of the microwave pulses used in these experiments normally leads to transitions within ±20 G of the magnetic field setting. However, incorporation of this pulse width in a simulation was found to have almost no effect on the intensities or frequencies of the spectral components. Therefore, all simulations were carried out using only a single input resonance magnetic field, in order to hasten the simulations.

[6] Only the O–O orientation of species II (Hori et al., 1980, 1982) based on cryogenic temperature single-crystal EPR measurements and that obtained from room temperature EPR measurements of oxyCo sperm whale Mb (Hori et al., 1980, 1982) are considered.

[7] The assignment of q_{zz} for the proximal histidyl N_ϵ in oxyCo globins as along the N_ϵ sp^2 hybrid, on the basis of X-ray crystallographic and nuclear quadrupole resonance spectroscopic studies of diamagnetic transition metal–pyridine/imidazole complexes (Hsieh et al., 1977; Ashby et al., 1978), is reasonable because this magnetic axis has been found by computer simulation of ESEEM spectra to be along a similar direction in low-spin complexes of ferric Mb (Magliozzo & Peisach, 1993).

[8] The expression $q_{zz} \wedge g_z$ etc., represents the angle between q_{zz} and g_z, and so forth.

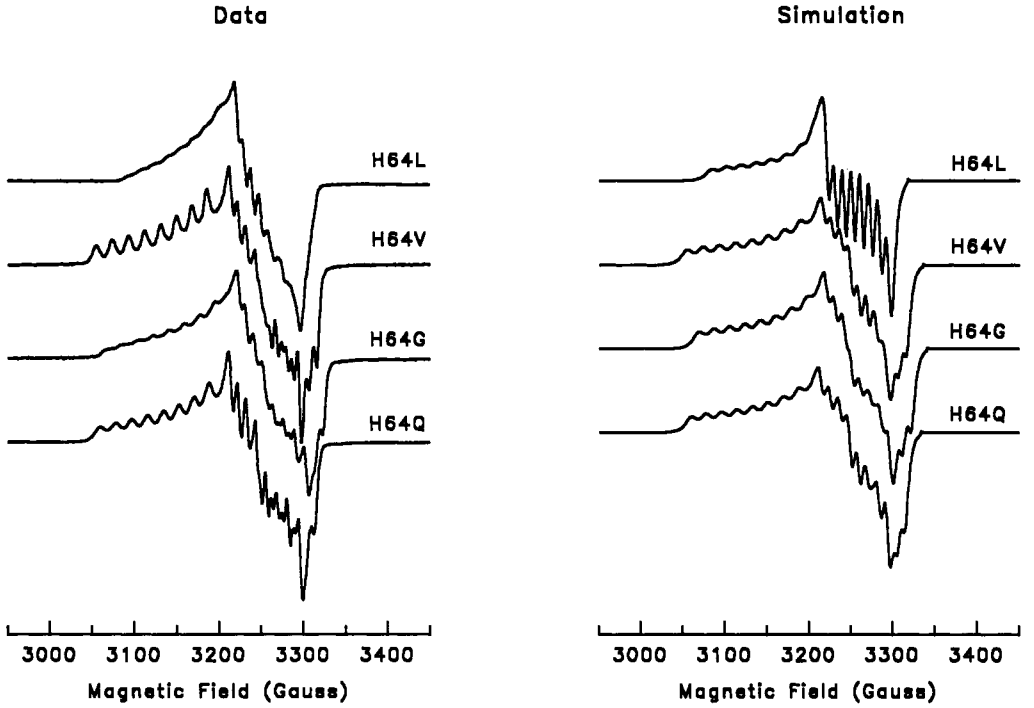

FIGURE 2: Frozen solution EPR spectra of oxyCo mutant human Mb: data (left panel) and simulation (right panel). The samples contain 0.6–0.8 mM protein in 67 mM Hepes, in D_2O at pH 7. Deuterium concentration is 60 atom%. Experimental conditions are microwave frequency = 9.09 GHz, power = 5 mW, modulation frequency = 100 KHz, modulation amplitude = 5 G, temperature = 77 K. Simulation parameters are summarized in Table 2.

Table 2: EPR Parameters of OxyCo Mutant and Wild-Type Human Mb

Mb	g_1	g_2	g_3	A_1^{Co} (MHz)	A_2^{Co} (MHz)	A_3^{Co} (MHz)
H64H(I)[a]	2.080	2.030	1.980	20.96	65.91	32.14
H64H(II)[a]	2.085	2.008	1.983	50.48	23.04	19.98
H64H(rt)[a]	2.056	2.011	2.003	52.13	31.29	20.46
H64Q[b]	2.085	2.001	1.983	53.00	32.00	25.00
H64G[b]	2.079	1.999	1.981	53.00	30.00	28.00
H64V[b]	2.086	2.001	1.982	56.00	30.00	25.00
H64L[b]	2.071	1.999	1.998	51.00	28.00	31.00

[a] Based on single-crystal EPR spectrum of oxyCo sperm whale Mb (Hori et al., 1980, 1982). I, II: species I and species II, respectively, in the single-crystal EPR spectrum at 77 K. rt: room temperature. [b] Computer simulation of frozen solution spectra.

Table 3: Superhyperfine Coupling Parameters for the N_ϵ of the Proximal Histidine in OxyCo Mb Mutants

mutants	A_{iso} (MHz)	r_{eff} (Å)	θ (deg)	ϕ (deg)	e^2qQ (MHz)	η	α (deg)	β (deg)	γ (deg)
H64H(I)[a]	2.57	3.60	21	0	2.13	0.37	90	21	0
H64H(II)[a]	2.57	3.60	17	0	2.13	0.40	0	17	0
H64H(rt)[a]	2.63	3.60	55	0	2.13	0.45	0	55	0
H64Q	2.84	3.40	40	0	2.24	0.40	90	40	0
H64G	2.88	3.40	50	0	2.21	0.40	70	50	0
H64V	3.20	3.60	20	0	2.31	0.42	0	20	0
H64L	3.79	3.60	0	0	2.62	0.59	0	0	0

[a] Euler and polar angles used are based on single-crystal EPR and X-ray crystallographic studies of oxyCo sperm whale Mb (Petsko et al., 1978; Hori et al., 1980, 1982) (see text). I, II: species I and II, respectively, in the single-crystal EPR spectrum at 77 K. rt: room temperature.

N_{III} axis and is almost perpendicular to the imidazole C_δ–C_ϵ axis. Thus, q_{yy} in oxyCo sperm whale Mb is almost perpendicular to g_x (the unpaired electron-containing π^* orbital of O_2), and $\alpha \approx 0°$. An angle of $\alpha > 0°$ therefore represents the rotation of the O–O bond above the heme normal from its position in oxyCo sperm whale Mb,[6] provided that the position of the proximal His is unchanged.

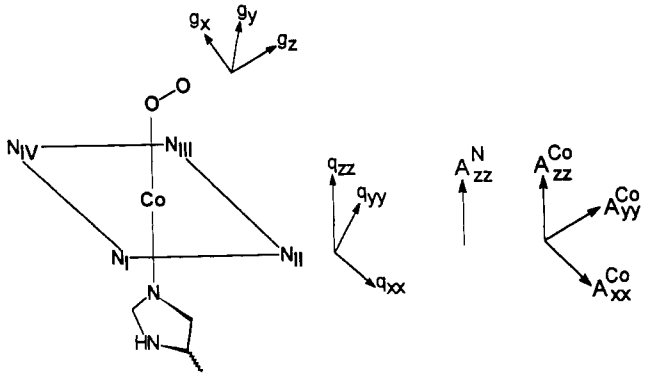

FIGURE 3: Schematic representation of the relative orientation of the g, ^{59}Co hyperfine, ^{14}N nuclear hyperfine, and ^{14}N nuclear quadrupole tensors in an oxyCo globin where the proximal histidyl imidazole C_δ–C_ϵ axis is along the pyrrole N_{II}–N_{IV} axis and the O–O axis is along the pyrrole N_I–N_{III} axis. The pyrrole numbering follows the convention of Fermi (1965).

Using computer simulations of frozen solution ESEEM spectra to estimate the Euler angles α, β, and γ as well as the polar angles θ_N and ϕ_N is normally achieved by fitting the relative intensities of the low-frequency lines and the lineshape of the broad, high-frequency line (McCracken et al., 1989; Cornelius et al., 1990). An accurate estimate of these angles requires that the coupling is sufficiently away from the exact cancellation condition (Flanagan & Singel, 1987) and/or that the relative intensities and/or frequencies of the low-frequency lines change sufficiently in data collected at different positions across the CW EPR absorption (Cornelius et al., 1990; Jiang et al., 1992; Magliozzo & Pesiach, 1993). Although such angle selection is generally minimal in oxyCo globins (Lee et al., 1992, 1993) due to the isotropic nature of the EPR absorption, as well as the near exact cancellation condition for the proximal histidyl N_ϵ, for the mutants, it is still possible to observe changes in the quality of the fits at one or more g values when the angles β, θ_N, and α are varied by 10°.

The ESEEM spectrum of H64L bears great similarity to that of oxyCo *Glycera* Hb (Lee et al., 1992) which also contains a Leu in the analogous position in the distal heme pocket. Simulation of the ESEEM spectrum of the human mutant (Table 3) requires slightly different coupling parameters than those found for the invertebrate protein (Lee et al., 1992). On the other hand, as in the case of oxyCo *Glycera* Hb, the best fit is obtained assuming alignment of all three magnetic tensors (Table 3).

Slightly different Euler angles are required to simulate the ESEEM spectra of H64G and H64Q (Table 3), despite their similarities. When the two sets of angles are interchanged, the quality of the fits at one or more g values is affected and the uncertainties increase. The simulations show a 2.2-MHz line of much higher relative intensity than its counterpart in the data. When the same sets of simulation parameters are used to generate spectra collected at longer τ values (for example, 3 times the proton periodicity), the fit in the intensity of this line improves. The splitting of the broad, high-frequency lines in these two spectra (Figure 1, right panel) cannot be simulated if the input θ_N is $\leq\beta - 20°$. This supports the assumption that the A_{zz}^N and q_{zz} are nearly coincident. If $\theta_N = 0°$ (or an angle much smaller than β) is used in the simulations, a value for r_{eff} of $\approx$2 Å is necessary to obtain a split broad line as found in the data. This dipole distance is much smaller than the X-ray crystal distance of $\approx$4 Å between the directly coordinated oxygen and the proximal histidyl N_ϵ (Petsko et al., 1978) and is thus unreasonable.

Attempts to fit the 1.26-MHz component observed in the spectrum of H64G (Figure 1, right panel) were unsuccessful. This feature was suppressed in data where a longer τ (for example, 3 times the proton periodicity) was used. It is possible that this feature arises from coupling to the pyrrole nitrogens. For example, in an ESEEM study of oxyCo[^{14}N]TPP-[^{15}N]-pyridine under similar experimental conditions (Magliozzo et al., 1987), low-frequency components are resolved at 0.4, 1.26, and 1.70 MHz.

Simulation of the ESEEM spectrum of H64V presents the greatest difficulty. The simulated spectrum shown in Figure 1 (left panel) utilized similar coupling parameters as those for H64G and H64Q but with the angles $\beta = \theta_N = 20°$, $\alpha = 0°$ (Table 3). The uncertainty in η[4], 0.33, is very large. If the angles $\beta = \Theta_N = 40°$, $\alpha = 0°$ are used, the spectrum at $g = 2.03$ (shown in Figure 1) can be fitted with $A_{iso} = 3.25$ MHz, $r_{eff} = 3.6$ Å, $e^2qQ = 2.2$ MHz, and $\eta = 0.41$. The uncertainties in A_{iso} and e^2qQ are similar to those found when $\beta = \theta_N = 20°$, $\alpha = 0°$ are used, while the uncertainty in η is reduced to 0.04. Although using larger angles reduces the uncertainty in η and fits the features at 1.45, 2.43, and 5.36 MHz at three experimental g values (1.99, 2.03, 2.08), the simulation generates a 0.66-MHz line at both $g = 2.03$ and $g = 2.08$, which is not resolved in the data. Therefore, the angles $\beta = \Theta_N = 20°$, $\alpha = 0°$ are utilized to generate the simulation spectrum presented in Figure 1.

Simulation of the ESEEM spectrum of the wild-type protein utilizes EPR parameters and information on Co–O–O bond geometry obtained from single-crystal EPR studies (Hori et al., 1980, 1982) and X-ray crystal structure (Petsko et al., 1978) of oxyCo sperm whale Mb. At cryogenic temperature, the single-crystal EPR spectrum of oxyCo sperm whale Mb contains two species (Chien & Dickinson, 1972; Dickinson & Chien, 1980; Hori et al., 1980, 1982). Species I is described by a Co–O–O bond angle ($g_{zz}^I \wedge A_{zz}^{Co}$)[8] of 159°, with the axis of the O–O bond (g_{zz}^I) over pyrrole II. Species II is described by a Co–O–O bond angle ($g_{zz}^{II} \wedge A_{zz}^{Co}$)[8] of 163°, with the axis of the O–O bond (g_{zz}^{II}) over pyrrole III (Petsko et al., 1978; Hori et al., 1980, 1982). In the simulation of the frozen solution ESEEM spectrum of the wild-type protein, A_{zz}^{Co}, A_{zz}^N, and q_{zz} are assumed to be coincident. Therefore, for species I, $\beta = \theta_N = 21°$ and $\alpha = 90°$ are used. For species II, $\beta = \Theta_N = 17°$ and $\alpha = 0°$ are used (Figure 3). The simulated spectrum shown in Figure 1 (left panel) was obtained with parameters for species II (Table 3). Simulation was also carried out using g values and Co–O–O bond angle information obtained from the room temperature single-crystal EPR spectrum of oxyCo sperm whale Mb (Hori et al., 1980, 1982). At room temperature, the Co–O–O bond ($g_{zz} \wedge A_{zz}^{Co}$)[8] is 125° and the O–O bond is over pyrrole III (Petsko et al., 1978; Hori et al., 1980, 1982). Therefore, the angles $\beta = \theta_N = 55°$, $\alpha = 0°$ are used in the ESEEM simulation. Simulation parameters of the wild-type protein, summarized in Table 3, using the three sets of g values and angles, are similar and close to those obtained for oxyCo sperm whale and horse Mb (Lee et al., 1992) ($A_{iso} = 2.46$ MHz, $e^2qQ = 2.15$ MHz, $\eta = 0.40$) using frozen solution EPR parameters described by Yonetani et al. (1974a).

ESEEM of OxyCo Mb Mutants in D_2O. ESEEM studies of oxyCo globins in D_2O can detect two populations of exchangeable deuterons (Lee et al., 1992, 1993). The first arises from the solvent or an ionizable side chain of nearby amino acids where the deuterons are dipole-coupled to the electron spin (Mims et al., 1990). These will give rise to a single ESEEM feature whose frequency is determined by the deuterium Zeeman energy. The second type consists of those hyperfine-coupled to the electron spin. In the ESEEM spectrum, these components will appear at frequencies given by:

$$\nu(^2H) = \nu(^2H)^{Larmor} \pm {}^1/_2|A_{eff}| \quad (6)$$

where A_{eff} is determined mainly by the hyperfine interaction since the deuterium quadrupole coupling is expected to be too small to contribute to the frozen solution spectrum (Mims & Peisach, 1989).

Figure 1 (middle panel) compares the ESEEM spectra of mutants and wild-type Mbs in D_2O with those of samples in H_2O (Figure 1, right panel) measured at similar experimental conditions. Spectra of H64L, H64V, and the wild-type protein are essentially identical in H_2O and D_2O at these experimental conditions.[9] For H64G and H64Q, the relative intensity of the 2.2 MHz line is higher in the D_2O spectrum than its counterpart in the H_2O spectrum. Since the ^2H Larmor frequency is at 1.96–2.00 MHz for these experimental magnetic field settings, the increase in the intensity of the 2.2-MHz line suggests the contribution of ^2H to the spectrum.

When the D_2O-exchanged wild-type protein was studied at 9.93 GHz, 3508 G (Figure 4A), two new peaks, not observed in the H_2O spectrum, were found at 2.28 and 2.55 MHz. The ^2H Larmor frequency at the experimental magnetic field setting is 2.28 MHz. When measurements were conducted at 9.33 GHz, 3349 G (Figure 4B), these peaks shifted to 2.19 and 2.46 MHz; the shifts, –0.09 MHz, match the change in ^2H Zeeman energy and allow the assignment of these lines to exchangeable ^2H. Therefore, the wild-type protein, like oxyCo sperm whale and horse Mb (Lee et al., 1992), contains a hyperfine-coupled ^2H with a coupling constant (A_{eff}, eq 6) of 0.6 MHz. This coupling, like that in the sperm whale and

[9] The same results are found when the deuterium concentration is raised to 90 atom % (see Materials and Methods).

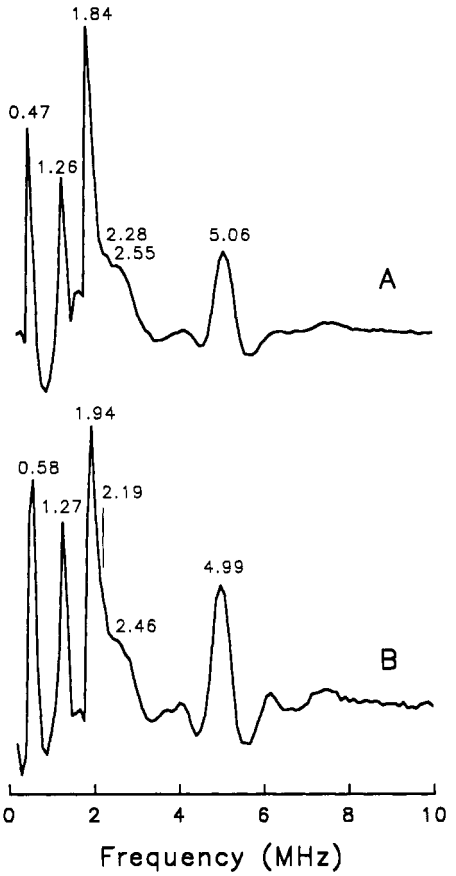

FIGURE 4: ESEEM of the wild-type protein in 67 mM Hepes, pH 7, in D_2O. Experimental conditions are (A) microwave frequency = 9.93 GHz, magnetic field = 3508 G, τ = 201 ns, temperature = 4.2 K, and (B) microwave frequency = 9.33 GHz, magnetic field = 3349 G, τ = 210 ns, temperature = 1.4 K.

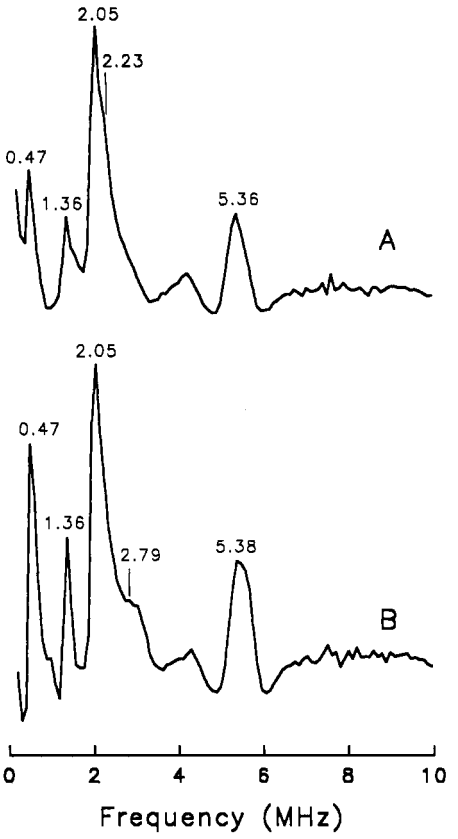

FIGURE 5: ESEEM spectra of H64Q in 0.1 M Hepes, pH 7, in D_2O. Experimental conditions are (A) microwave frequency = 10.12 GHz, magnetic field = 3562 G, τ = 198 ns, temperature = 4.2 K, and (B) microwave frequency = 10.12 GHz, magnetic field = 3632 G, τ = 194 ns, temperature = 4.2 K.

horse proteins, is observed at three experimental g values, 1.99, 2.03, and 2.08.

ESEEM measurements of D_2O-exchanged samples of H64G and H64Q were repeated at 10.12 GHz. Figure 5 shows the spectra of H64Q in D_2O as an illustration. At g = 2.03 (Figure 5A) and g = 2.08, a 2.23-MHz peak, close to the ^2H Larmor frequency (2.33 MHz) at the experimental magnetic field setting, is resolved. At g = 1.99 (Figure 5B), a broad peak, not observed in H_2O, is resolved at ≈2.79 MHz. This 2.79-MHz feature is also present in spectra obtained at 9.8 GHz (also only at g = 1.99) but not at 8.5 GHz (Figure 1, left panel), while the feature assigned to the ^2H Larmor line moves with the change in ^2H Zeeman energy. Therefore, it is not possible to assign the 2.79-MHz feature observed at 10.12 GHz (Figure 4B) as arising from ^2H, and it is concluded that no hyperfine-coupled ^2H can be detected for H64Q. For H64G, only the ^2H Larmor frequency was resolved in data collected at various microwave frequencies.[9]

When data were collected at 9.38 GHz, the D_2O spectrum of H64L remained identical to the H_2O spectrum measured under similar conditions. Unlike oxyCo *Glycera* Hb (Lee et al., 1992), no ^2H Larmor frequency was resolved. At this microwave frequency, the D_2O spectrum of H64V shows a small broadening at the high-frequency end of the 1.45-MHz line. Dividing the D_2O data by the H_2O data (Mims, 1984), a method for isolating the ^2H components from the ^{14}N features (Lee et al., 1992), finds a 1.94-MHz line, while the ^2H Larmor frequency at the experimental magnetic field setting is 2.16 MHz. However, the intensity of this 1.94-MHz component is not significantly higher than the base-line noise level and cannot be unambiguously assigned to exchangeable ^2H.[9] No measurements were repeated at higher microwave frequencies for these two mutants because an increase in magnetic field strength will only shift any ^2H components, if present, toward the broad 2.4-MHz ^{14}N line in H64V (or the 3.1-MHz line in H64L) and detection of ^2H components is expected to be more difficult.[10]

DISCUSSION

Electron-Nuclear Hyperfine Coupling. Hyperfine coupling to the proximal His occurs through induced unpaired spin density in the fully occupied d_z^2 orbital of Co (Wayland & Abe-Elmageed, 1974; Tovrog et al., 1976) and can be affected by changes in the electronic structure of the Co–O_2 bond. This bond can be perceived electronically in a valence bond description as varying between Co^{2+}–O_2 and Co^{3+}–$O_2^{\bullet-}$ (Tovrog et al., 1976). A shift toward the Co^{3+}–$O_2^{\bullet-}$ structure will raise the relative energy of the Co d_z^2 orbital, decrease induced unpaired electron spin density in this orbital, and subsequently reduce the hyperfine coupling to the proximal His ligand.

Hyperfine coupling to the proximal His in wild-type and mutant oxyCoMb decreases in the order: H64L > H64V ≥ H64G ≈ H64Q > wild-type (Table 3). Assuming that the mutants differ only in the nature of their E7 residues, the alterations in hyperfine couplings can be rationalized by examining the effect of the E7 residue on the ionic character of the Co–O_2 bond. A residue having a polar side chain can

[10] The spectra presented in Figure 1 are collected at microwave frequencies of 8.5 GHz, which is the lower limit available in our laboratory.

stabilize the ionic character of that bond. Gln has a more polar side chain than Leu or Val. The smaller hyperfine coupling found for the proximal His of H64Q is consistent with the idea that its oxyCo unit, being in a more polar environment, is more ionic.

The trend of hyperfine couplings found for the proximal His of the Leu, Val, and Gly mutants, H64L > H64V > H64G, can also be correlated with the differences in polarity of the side chains of the E7 residues. Side-chain polarity of Leu, Val, and Gly is measured by the ΔG (normalized with that for Gly = 0 kcal/mol) required for transferring the side chains from ethanol (a model for nonpolar solvent) to water (a typical polar solvent) and is estimated as +2.4 kcal/mol for Leu and +1.7 kcal/mol for Val (Cantor & Schimmel, 1980). Therefore, the bound O_2 in H64L, H64V, and H64G is subjected to an environment of increasing polarity across the series, thereby leading to an increase in the ionic character of the Co–O_2 bond. The observed reduction in hyperfine coupling to the proximal His is therefore reasonable.

Hyperfine coupling to the proximal His is smallest in the wild-type protein. Like oxyCo sperm whale Mb (Lee et al., 1992), the recombinant wild-type human Mb is shown by our ESEEM study in D_2O to contain a hydrogen bond between the E7 His and the bound O_2. The acidic proton on the distal histidyl imidazole, being an electrophile, stabilizes the Co^{3+}–$O_2^{\bullet-}$ structure and will lead to a decrease in hyperfine coupling to the proximal ^{14}N ligand. Previously, a 1.2-MHz difference in hyperfine coupling to the proximal ligand was found between oxyCo sperm whale or horse Mb and oxyCo *Glycera* Hb (Lee et al., 1992). The latter has a Leu, instead of a His, at the E7 position and thus cannot form a hydrogen bond to the bound O_2. However, the lack of a hydrogen bond in oxyCo *Glycera* Hb cannot fully account for the 1.2-MHz difference in coupling. The hydrophobicity of the Leu side chain should also be taken into consideration. This is apparent by the 0.3 → 0.6-MHz difference in the coupling between the wild-type and the Gln, Gly, and Val mutants (Table 3). In oxyCo soybean leghemoglobin, where the E7 residue is also a His and there is a pH-dependent hydrogen bond to O_2, the difference in hyperfine coupling between the hydrogen-bonded form and the non-hydrogen-bonded form is only 0.7 MHz (Lee et al., 1993).

Nuclear Quadrupole Coupling. The nuclear quadrupole coupling constant, e^2qQ, for the proximal histidyl N_ϵ is determined by the electric field gradient along its lone-pair-containing sp^2 hybrid (Hsieh et al., 1977; Ashby et al., 1978). Increase in lone-pair donation to the Co d_{z^2} orbital will decrease the efg along this hybrid and decrease the nuclear quadrupole coupling. For oxyCo globins, the extent of lone-pair donation from the proximal histidyl N_ϵ should increase with the increase of positive charge on Co. Therefore, the nuclear quadrupole coupling will decrease with an increase in the ionic character of the Co–O_2 bond.

The trend in nuclear quadrupole coupling for the oxyCo Mb mutants parallels that of hyperfine coupling, H64L > H64V ≥ H64G ≈ H64Q, and can be rationalized as being due to the differences in the polarity of the E7 residue side chain as discussed above. Similarly, a hydrogen bond between bound O_2 and the E7 His in the wild-type increases the positive charge on Co and leads to an increase in lone-pair donation from the proximal histidyl N_ϵ and a decrease in quadrupole coupling. Therefore, both hydrogen bonding to bound O_2 and a polar protein environment surrounding the bound O_2 can increase overlap between the metal and the *trans* ligand, the proximal histidyl imidazole. This ESEEM study has thus demonstrated

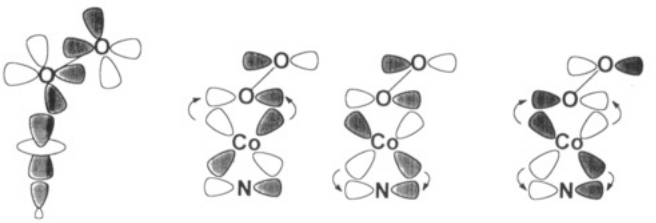

FIGURE 6: Schematic representation of (A) the σ-bonding and (B) and (C) the π-bonding in an oxyCo globin. For π-bonding, only the unpaired-electron containing π^* orbital of O_2 is considered here. (B) The O–O axis is parallel to the proximal histidyl N_ϵ $p\pi$ orbital such that the two axial ligands π bond with different Co $d\pi$ orbitals. (C) The O–O axis is perpendicular to the N_ϵ $p\pi$ orbital or parallel to the imidazole plane such that the two axial ligands π bond with the same Co $d\pi$ orbital.

how the two axial bonds in a six-coordinate Co(II) complex can be modulated by the environment of one of the axial ligands. An increase in ionicity of one axial bond leads to an increase in the covalency of the *trans* metal–ligand bond. ESEEM studies of oxyCo globins of different distal heme environments have thus allowed for an evaluation of the effects of different dielectrics on metal–ligand bonds.

The asymmetry factor, η (eq 3), is determined by both σ- and π-bonding effects and is more difficult to predict. Since both Co $d\pi$ orbitals are fully occupied, π-bonding is predominantly a $d\pi \rightarrow$ ligand π interaction (Dedieu et al., 1976). Co $d\pi \rightarrow N_\epsilon$ $p\pi$ donation will be maximized when the imidazole π system and the O_2 unpaired-electron-containing π orbital are perpendicular to each other (Figure 6B), for example, in the case of oxyCo sperm whale Mb (Hori et al., 1980, 1982).[6] On the other hand, rotation of the O–O bond by 90° above the heme normal will result in interaction of the two axial ligand π systems with the same Co $d\pi$ system (Figure 6C), possibly in the case of H64G and H64Q. However, a similar value for η is found for H64G, H64Q, and the wild-type protein. It is likely that any change in π-bonding is compensated for by a change in σ-bonding.

Geometry of the Bound O_2. Simulation of the ESEEM spectra requires large values for $\beta = \theta_N$ and α for H64G and H64Q but not for H64L and H64V (Table 3). It is reasonable to conclude that the Co–O–O bond in H64G and H64Q is bent (Co–O–O bond angle < 180°), similar to that in oxyCo sperm whale Mb (and presumably the human wild-type) at room temperature (Hori et al., 1980, 1982). The O–O bond in these two mutants may have rotated above the heme normal, and its projection on the heme plane is no longer parallel to the pyrrole N_I–N_{III} axis as in oxyCo sperm whale Mb[6] (Petsko et al., 1978; Hori et al., 1980, 1982). On the other hand, the ESEEM spectra of H64L and H64V can be simulated with very small Euler (and polar) angles (Table 3). It is possible that the Co–O–O bond is more obtuse than that in oxyCo sperm whale Mb at room temperature.

The Co–O–O bond angles found for the mutant and wild-type Mbs can be used to assess the role of the E7 residue on bond geometry. This residue in the mutants cannot be a hydrogen bond donor to bound O_2, and yet, the Co–O–O bond angle in H64G and H64Q is similar to that in oxy Co sperm whale Mb (Petsko et al., 1978) (and the human wild-type). Therefore, hydrogen bond donor strength of the E7 histidine cannot be taken to be responsible for the bent metal–O–O bond in oxyCoMb (Petsko et al., 1978) and oxyFeMb (Phillips, 1980). As noted in a review of this paper, this observation is not unexpected since the Co–O–O bond in Co(acacen)-

(py)(O_2) (Calligàris, 1973) and the Fe–O–O bond in Fe(TPivP)(N-MeIm)(O_2) (Collman et al., 1974, 1975) are bent, while a hydrogen bond to bound O_2 in these compounds is either absent or, in the latter case, very weak. Rather, the electronic configuration of the Co–O–O unit predicts a bent Co–O–O geometry, and analogy can be drawn to the structural studies of Co-nitrosyl complexes by Enemark & Feltham (1972, 1974a,b). These workers found a Co–N–O bond angle of 135° for $[Co^{3+}\text{-}(NO)^{-}]^{2+}$ and 179° for $[Co^{1+}\text{-}(NO)^{+}]^{2+}$. It appears that the Co–N–O angle decreases with an increase in negative charge on the nitrosyl ligand. It is interesting to note that the present ESEEM study finds a smaller Co–O–O bond angle for the Mbs that contain a more ionic Co–O_2 bond, with increased negative charge on the O_2 ligand, due to the presence of a more polar E7 residue. To this extent, the geometry of the Co–O–O bond in oxyCo globins follows a similar trend observed for Co–NO complexes and an increase in the polarity of the E7 side chain may lead to a less obtuse Co–O–O bond.

The relationship between the size of the E7 residue and the Co–O–O bond angle is also evaluated, since the distal pocket has always been perceived as a restricted cavity and the side-chain volume of the residues closest to the sixth coordination position of the heme may be important in deciding the metal–O–O bond angle. Considering the variation in the size between the Gly "side chain" and those of Gln, Val, Leu, and His, one would expect that the Co–O–O bond would be the most linear in H64G, but this is not found to be the case. Therefore, there does not seem to be any fast relationship between the side-chain volume of the E7 residue and the metal–O–O bond angle.

Hyperfine Coupling to Exchangeable ^2H. D_2O-induced narrowing of ^{59}Co hyperfine features in CW EPR spectra has been used as a probe for a hydrogen bond between the distal His and bound O_2 in oxyCo globins (Yonetani et al., 1974b; Ikeda-Saito et al., 1978, 1981). In previous CW EPR studies of oxyCo mutant Mbs in D_2O, such D_2O effects were observed in the spectra of H64Q, H64V (Ikeda-Saito et al., 1991), and H64G (Dou et al., unpublished data). Since for H64V and H64G no hydrogen bond between the bound O_2 and the E7 distal residue is possible, it is concluded that the detection of D_2O-induced narrowing of Co hyperfine lines in the CW EPR spectra of oxyCo globins is not always an indication of the presence of a hydrogen bond between the bound O_2 and the distal E7 residue (Ikeda-Saito et al., 1991). The absence of ^2H components other than the Larmor frequency in the ESEEM spectra of D_2O-exchanged H64V and H64G supports this conclusion. This is also supported by an ESEEM study of oxyCo leghemoglobin at neutral pH (Lee et al., 1993) which shows the absence of a hydrogen bond to bound O_2 at neutral pH despite the presence of a small D_2O effect in the CW EPR spectrum (Ikeda-Saito et al., 1981). Therefore, D_2O-induced narrowing of the Co hyperfine lines in the CW EPR spectrum of oxyCo globins can only be used to evaluate proximity of exchangeable deuterons and does not necessarily indicate hydrogen bonding to bound O_2.

The present ESEEM results also cannot substantiate the previously proposed hydrogen bond between bound O_2 and the E7 glutamine in H64Q (Ikeda-Saito et al., 1991), although a hydrogen bond between this residue and the heme-bound ligands in the ferric derivatives of H64Q has been reported (Ikeda-Saito et al., 1992). Similar hydrogen bonds have also been reported for ferric elephant Mb (Krishnamoorthi et al., 1984; Vyas et al., 1993) which also contains a Gln (Gln 64) at position E7. Kinetic studies show that E7 Gln stabilizes the oxy form of sperm whale ferrous H64Q as compared to the E7 Leu, Val, and Gly mutants, albeit to a smaller extent than the distal histidine in the oxyferrous wild-type sperm whale Mb (Rohlfs et al., 1990). The faster O_2-dissociation rate found for oxyFe sperm whale H64Q as compared to that for the wild-type protein can be due to the lack of a hydrogen bond between Gln 64 and the bound O_2 in the mutant.

Table 4: O_2-Binding Parameters of Mutant and Wild-Type Myoglobins

oxyCo-substituted human Mbs[a,b]		Fe sperm whale Mbs[c]			
protein	P_{50} (Torr)	protein	k_{on} ($\times 10^{-6}$ M^{-1} s^{-1})	k_{off} (s^{-1})	$k_{association}$ ($\times 10^{-6}$ M^{-1})
H64H	30	H64H[d]	16	17	0.9
H64Q	25	H64Q[e]	24	130	0.185
H64V	>1300	H64G[d]	140	1600	0.088
H64L	>1300	H64V[d]	250	23000	0.011
		H64L[d]	98	1600	0.023

[a] Ikeda-Saito et al. (1991). [b] 15 °C, pH 7. [c] 20 °C, pH 7. [d] Rohlfs et al. (1990). [e] Carver et al. (1990).

Electronic Structure and O_2 Affinity. The present ESEEM study of oxyCo human Mbs reveals electronic structures that can be correlated with the polarity of the E7 residues. O_2-binding parameters of the various Co human Mb mutants (Ikeda-Saito et al., 1991) and those of the corresponding Fe sperm whale Mbs (Carver et al., 1990; Rohlfs et al., 1990) (Table 4) have also been shown to be related to the polarity of the E7 residues. An increase in O_2 affinity is found for Mbs that contain a more polar E7 residue. It is interesting to note that the trend for electron-nuclear coupling to the proximal His in the Co human Mb (Table 3) is paralleled by that for O_2 affinity of the Fe sperm whale Mbs (Table 4). An increase in electron-nuclear coupling is accompanied by an increase in O_2 affinity, as was suggested in a comparative ESEEM study of oxyCo sperm whale and horse Mb and oxyCo *Glycera* Hb (Lee et al., 1992). Rohlfs et al. (1990) propose that the equilibrium constant for O_2 binding is determined by the ability of the E7 residue to stabilize the polar Fe–O_2 complex. In this study, we demonstrate that the polarity of the E7 residue increases the ionic character of the Co–O_2 bond, using electron-nuclear coupling to the proximal His as a probe of degree of ionicity. To this extent, the electronic structures of the Co proteins correspond to those of the analogous Fe proteins and correlate with functional properties.

ACKNOWLEDGMENT

We thank Dr. S. G. Boxer (Stanford University) for the human Mb expression system and the reviewer who brought to our attention the works of Enemark and Feltham.

REFERENCES

Ashby, C. I. H., Cheng, C. P., & Brown, T. L. (1978) *J. Am. Chem. Soc. 100*, 6057.
Belford, R. L., & Nilges, M. J. (1979) Presented at the International Electron Paramagnetic Resonance Symposium, 21st Rocky Mountain Conference, Denver, CO.
Britt, R. D., & Klein, M. P. (1987) *J. Magn. Reson. 74*, 535.
Calligàris, M. (1973) *Inorg. Nucl. Chem. Lett. 9*, 419.
Cantor, C. R., & Schimmel, P. R. (1980) *Biophysical Chemistry*, Part I, 52, W. H. Freeman & Co., New York.
Carver, T. E., Rohlfs, R. J., Olson, J. S., Gibson, Q. H., Blackmore, R. S., Springer, B. A., & Sligar, S. G. (1990) *J. Biol. Chem. 265*, 20007.
Chien, J. C. W., & Dickinson, L. C. (1972) *Proc. Natl. Acad. Sci. U.S.A. 69*, 2783.

Collman, J. P., Gague, R. R., Reed, C. A., Robinson, W. T., & Rodley, G. A. (1974) *Proc. Natl. Acad. Sci. U.S.A. 71*, 1326.
Collman, J. P., Gague, R. R., Reed, C. A., Halbert, T. R., Land, G., & Robinson, W. T. (1975) *J. Am. Chem. Soc. 97*, 1427.
Cornelius, J. B., McCracken, J., Clarkson, R. B., Belford, R. L., & Peisach, J. (1990) *J. Phys. Chem. 94*, 6977.
Dalvit, C., & Wright, P. E. (1987) *J. Mol. Biol. 194*, 313.
Dedieu, A., Rohmer, M.-M., & Veillard, A. (1976) *J. Am. Chem. Soc. 98*, 5789.
Dickerson, R. E., & Geis, I. (1983) *Hemoglobin: Structure, Function, Evolution, and Pathology*, The Benjamin/Cummings Publishing Company, Inc., Menlo Park, CA.
Dickinson, L. C., & Chien, J. C. W. (1980) *Proc. Natl. Acad. Sci. U.S.A. 77*, 1235.
Enemark, J. H., & Feltham, R. D. (1972) *Proc. Natl. Acad. Sci. U.S.A. 69*, 3534.
Enemark, J. H., & Feltman, R. D. (1974a) *J. Am. Chem. Soc. 96*, 5002.
Enemark, J. H., & Feltman, R. D. (1974b) *J. Am. Chem. Soc. 96*, 5004.
Fermi, G. (1975) *J. Mol. Biol. 97*, 237.
Flanagan, H. L., & Singel, D. J. (1987) *J. Chem. Phys. 87*, 5606.
Hoffman, B. M., & Petering, D. H. (1970) *Proc. Natl. Acad. Sci. U.S.A. 67*, 637.
Hoffman, B. M., Diemente, D. L., & Basolo, F. (1970) *J. Am. Chem. Soc. 92*, 61.
Hori, H., Ikeda-Saito, M., & Yonetani, T. (1980) *Nature 288*, 501.
Hori, H., Ikeda-Saito, M., & Yonetani, T. (1982) *J. Biol. Chem. 257*, 3636.
Hsieh, Y.-N., Rubenacker, G. V., Cheng, C. P., & Brown, T. L. (1977) *J. Am. Chem. Soc. 99*, 1384.
Hunt, L. T., Hurst-Calderone, S., & Dayhoff, M. O. (1978) in *Atlas of Protein Sequence and Structure* (Dayhoff, M. O., Ed.) 5th ed., pp 229–249, National Biomedical Research Foundation, Washington.
Ikeda-Saito, M., Iizuka, T., Yamamoto, H., Kayne, F. J., & Yonetani, T. (1977) *J. Biol. Chem. 252*, 4882.
Ikeda-Saito, M., Hori, H., Inubushi, T., & Yonetani, T. (1981) *J. Biol. Chem. 256*, 10267.
Ikeda-Saito, M., Lutz, R. S., Shelley, D. A., McKelvey, E. J., Materra, R., & Hori, H. (1991) *J. Biol. Chem. 266*, 23641.
Ikeda-Saito, M., Hori, H., Andersson, L. A., Prince, R. C., Pickering, I. J., George, G. N., Sanders, C. R., II, Lutz, R. S., McKelvey, E. J., & Mattera, R. (1992) *J. Biol. Chem. 267*, 22843.
Jiang, F., McCracken, J., Peisach, J. (1990) *J. Am. Chem. Soc. 112*, 9035.
Jiang, F., Conry, R. R., Bubacco, L., Tyeklar, Z., Jacobson, R. R., Karlin, K. D., & Peisach, J. (1993) *J. Am. Chem. Soc. 115*, 2093.
Krishnamoorthi, R., La Mar, G. N., Mizukami, H., & Romero, A. (1984) *J. Biol. Chem. 259*, 8826.
Lee, H. C., Ikeda-Saito, M., Yonetani, T., Magliozzo, R. S., & Peisach, J. (1992) *Biochemistry 31*, 7274.
Lee, H. C., Wittenberg, J. B., & Peisach, J. (1993) *Biochemistry 32*, 11500.
McCracken, J., Peisach, J., & Dooley, D. M. (1987) *J. Am. Chem. Soc. 109*, 4064.
McCracken, J., Pember, S., Benkovic, S. J., Villafranca, J. J., Miller, R. J., & Peisach, J. (1988) *J. Am. Chem. Soc. 110*, 1069.
Magliozzo, R. S., & Peisach, J. (1993) *Biochemistry 32*, 8446.
Magliozzo, R. S., McCracken, J., & Peisach, J. (1987) *Biochemistry 26*, 7923.
Maurice, A. M. (1981) Ph.D. Thesis, University of Illinois, Urbana, IL.
Mims, W. B. (1984) *J. Magn. Reson. 59*, 291.
Mims, W. B., & Peisach, J. (1978) *J. Chem. Phys. 69*, 4921.
Mims, W. B., & Peisach, J. (1989) in *Advanced EPR Applications in Biology and Biochemistry* (Hoff, A. J., Ed.) p 1, Elsevier Press, Holland.
Mims, W. B., Davis, J. L., & Peisach, J. (1990) *J. Magn. Reson. 86*, 273.
Nilges, M. J. (1979) Ph.D. Thesis, University of Illinois, Urbana, IL.
Olson, J. S., Mathews, A. J., Rohlfs, R. J., Springer, B. A., Egeberg, K. D., Sligar, S. G., Tame, J., Renaud, J.-P., & Nagai, K. (1988) *Nature 336*, 265.
Peisach, J., Mims, W. B., & Davis, J. L. (1979) *J. Biol. Chem. 254*, 12379.
Petsko, G. A., Rose, D., Tsernoglou, D., Ikeda-Saito, M., & Yonetani, T. (1978) in *Frontiers of Biological Energetics* (Dutton, P. L., Scarpa, A., & Leigh, J. S., Jr., Eds.) p 1011, Academic Press, New York.
Phillips, S. E. V. (1980) *J. Mol. Biol. 142*, 531.
Rohlfs, R. J., Mathews, A. J., Theodore, T. E., Olson, J. S., Springer, B. A., Egeberg, K. D., & Sligar, S. G. (1990) *J. Biol. Chem. 265*, 3168.
Savicki, J. P., Lang, G., & Ikeda-Saito, M. (1984) *Proc. Natl. Acad. Sci. U.S.A. 81*, 5417.
Tovrog, B. S., Kitko, D. J., & Drago, R. S. (1976) *J. Am. Chem. Soc. 98*, 5144.
Vyas, K., Rajarathnam, K., Yu, L. P., Emerson, S. D., La Mar, G. N., & Krishnamoorthi, R. (1993) *J. Biol. Chem. 268*, 14826.
Wayland, B. B., & Abd-Elmageed, M. E. (1974) *J. Am. Chem. Soc. 96*, 4809.
Yonetani, T., Yamamoto, H., Iizuka, T. (1974a) *J. Biol. Chem. 249*, 2168.
Yonetani, T., Yamamoto, H., & Woodrow, G. V., III. (1974b) *J. Biol. Chem. 249*, 682.
Yu, N.-T. (1986) *Methods Enzymol. 130*, 350.